Cytoskeletal tension regulates mesodermal spatial organization and subsequent vascular fate

Quinton Smith[a,b,c,1], Nash Rochman[a,b,c,1], Ana Maria Carmo[a,b,c], Dhruv Vig[a,b,c], Xin Yi Chan[a,b,c], Sean Sun[b,c,d,2], and Sharon Gerecht[a,b,c,e,2]

[a]Department of Chemical and Biomolecular Engineering, Johns Hopkins University, Baltimore, MD 21218; [b]Physical Sciences-Oncology Center, Johns Hopkins University, Baltimore, MD 21218; [c]The Institute for NanoBioTechnology, Johns Hopkins University, Baltimore, MD 21218; [d]Department of Mechanical Engineering, Johns Hopkins University, Baltimore, MD 21218; and [e]Department of Materials Science and Engineering, Johns Hopkins University, Baltimore, MD 21218

Edited by Robert Langer, MIT, Cambridge, MA, and approved July 5, 2018 (received for review May 23, 2018)

Morphogenesis during human development relies on the interplay between physiochemical cues that are mediated in part by cellular density and cytoskeletal tension. Here, we interrogated these factors on vascular lineage specification during human-induced pluripotent stem-cell (hiPSC) fate decision. We found that independent of chemical cues, spatially presented physical cues induce the self-organization of Brachyury-positive mesodermal cells, in a RhoA/Rho-associated kinase (ROCK)-dependent manner. Using unbiased support vector machine (SVM) learning, we found that density alone is sufficient to predict mesodermal fate. Furthermore, the long-withstanding presentation of spatial confinement during hiPSC differentiation led to an organized vascular tissue, reminiscent of native blood vessels, a process dependent on cell density as found by SVM analysis. Collectively, these results show how tension and density relate to vascular identity mirroring early morphogenesis. We propose that such a system can be applied to study other aspects of the stem-cell niche and its role in embryonic patterning.

support vector machine learning | stem cells | differentiation | vascular biology

Momentous efforts motivated by developmental insight have demonstrated that the combination of chemical cues, presentation of defined extracellular microenvironments, and population-specific enrichment steps can lead to directed differentiation protocols capable of generating specific cellular populations from human-induced pluripotent stem cells (hiPSCs) that stem from all three germ layers (1–3). Nonetheless, our understanding of how the complex interplay among various cues directs hiPSC differentiation events is incomplete. Furthermore, means to analyze, interpret, and predict the roles of complex niches in a robust and unbiased manner are critical to the promise of stem-cell technology in a clinical setting. Support vector machine (SVM) learning, a robust binary segmentation algorithm, is a powerful tool for both data-driven prediction and the unbiased identification of important/causative experimental variables. SVMs have been implemented in the automated classification and prediction of phenotypic and genotypic characteristics of many cellular populations (4), including the classification of cancer phenotypes for clinical applications (5) as well as the optimization of microenvironments to control stem-cell pluripotency and differentiation (6–8).

The use of micropatterning tools has led to the generation of highly reproducible "gastruloids," where spatial organization during embryonic gastrulation can be mimicked in vitro, offering a robust system to evaluate the roles of the stem-cell niche during early and late-stage differentiation events. Seminal work from Warmflash et al. (9) demonstrates how prepatterned hPSC colonies grown on circular micropatterned domains undergo gastrulation-like events, expressing markers from mesoderm, endoderm, ectoderm, and trophectoderm lineages, in a spatially dependent manner upon the stimulation of bone morphogenetic protein-4 (BMP-4). This size-dependent, radially symmetric pattern formation is generated by the ability of hPSCs to sense and interpret the edge of the imposed geometric cues by differentially expressing key BMP-4 receptors in a density-dependent manner (10). Consequently, this varied receptor presentation propagates a Turing-like reaction–diffusion mechanism, resulting in a positive–negative feedback loop between BMP-4 and its inhibitor NOGGIN, that can predict patterned fate acquisition in circular domains using computational approaches (11, 12). We have monitored the loss of pluripotency of hiPSCs seeded on circular micropatterns and found that differentiation occurs in a bimodal fashion, where cells seeded on small micropattern domains either completely differentiate or maintain pluripotent marker expression over the course of 5 d. From these experiments using Monte Carlo simulations, we were able to describe this stochastic biphasic differentiation modality (13).

While these approaches have provided vast insight into the role of soluble and geometric cues on early differentiation events, there are few studies that explore the role of long-term administration of confinement on lineage specification. For example, it has been shown that prolonged confinement leads to the self-organization of cardiac microchambers, amenable to drug toxicity studies (14). Our own recent work has shown that

Significance

Human-induced pluripotent stem cells (hiPSCs) offer an opportunity to study how the developing embryo twists, folds, and expands into a collection of highly self-organized tissues. Introducing varying degrees of confinement with surface micropatterning may drive self-organization into tissues that mirror the structure and complexity of the embryo in vitro. Using high-throughput image-processing and machine-learning algorithms, we studied the relationships between cytoskeletal tension, density, and micropattern geometry on the ability to predict pattern formation in early and late-stage hiPSC maturation toward vascular lineages. We find that the combination of these approaches unveils the importance of cell density and cytoskeletal tension in how hiPSCs sense their environment and differentiate to the mesodermal lineage toward vascular fates.

Author contributions: Q.S., N.R., D.V., S.S., and S.G. designed research; Q.S., A.M.C., and X.Y.C. performed research; N.R. and D.V. contributed new reagents/analytic tools; Q.S., N.R., A.M.C., D.V., S.S., and S.G. analyzed data; and Q.S., N.R., S.S., and S.G. wrote the paper.

The authors declare no conflict of interest.

This article is a PNAS Direct Submission.

[1]Q.S. and N.R. contributed equally to this work.

[2]To whom correspondence may be addressed. Email: ssun@jhu.edu or gerecht@jhu.edu.

This article contains supporting information online at www.pnas.org/lookup/suppl/doi:10.1073/pnas.1808021115/-/DCSupplemental.

Published online July 23, 2018.

mesodermal populations are sensitive to spatial confinement during vascular specification (15). Micropatterning tools have further uncovered the role of the cytoskeleton during differentiation through analysis of how RhoA/Rho-associated kinase (ROCK) impacts actomyosin contractility in MSCs undergoing fate decision toward adipocyte and osteocyte lineages (16–19). Nonetheless, these studies rely on the presence of soluble cues, while studies exploring the undeveloped cytoskeletal structure of hiPSCs, as it relates to their differentiation capacity, have been relatively unexplored (20, 21). Here we utilized micropatterning to show how the interplay between cytoskeletal tension (i.e., active forces developed by the cell) and local cell density, reported as the fraction of each local region occupied by nuclei, modulates mesodermal fate independently of soluble cues, which subsequently leads to vascular commitment from hiPSCs.

Here we hypothesize that cytoskeletal tension and local cell density modulates mesodermal fate and subsequent vascular commitment from hiPSCs. To test this hypothesis, rather than culture pluripotent colonies on circular domains before differentiation (9, 11, 12, 14), we used an approach in which hiPSCs are seeded as a single-cell suspension on an array of micropatterned geometries, which are allowed to undergo mesoderm induction followed by vascular specification. In this manner, cells are not preconditioned by the patterns and are randomly adhered to the surface where they interact with varying geometries at the onset of differentiation. Thus, we do not expect the generation of a well-defined gradient in stimulatory and inhibitory signaling (such as BMP-4 or NOGGIN, respectively), while the differentiating cells proliferate and migrate to fill the confined geometries. Consequently, we propose that in this system, any self-organization events result from mechanical cues as differentiating cells encounter boundaries. In the absence of controlled morphogen gradients, we apply SVM learning to predict self-organization events as a function of cell density and cytoskeletal tension measured by the RhoA/ROCK pathway. We find that local geometry guides the organization of early mesodermal, Brachyury-positive (T+) cells that subsequently induces the downstream multicellular differentiation and organization of endothelial cells (ECs) and pericytes. Importantly, we find that we can predict the outcome of this spatially guided differentiation and vascular specification, solely from cell density and cytoskeletal tension.

Results

An Imaging–Patterning Modality Used to Predict Early Mesoderm with SVM Learning. The mesoderm identified by transcription factor T arises from epithelial-to-mesenchymal transition events during gastrulation and forms tissues including the heart, muscle, and vasculature. While Turing-like systems can describe cellular spatial organization from the interaction of diffusible chemical species and stochastic fluctuations, the contribution of actomyosin activity and extracellular matrix (ECM) presentation has not been fully investigated. Using microfabrication tools, we sought to control cues administered by the ECM and monitor myosin II activity, a potent regulator of the cytoskeleton, in efforts to understand how these variables contribute to mesodermal specification (Fig. 1*A*). Micropatterns (manufactured by CYTOO) were designed to create multiple geometries (e.g., squares, triangles, stars, hexagons, etc.) of different sizes (Fig. 1 *B, i* and *SI Appendix*, Fig. S1). To prevent any morphogen cross-talk between the micropatterns, a gap distance of 200 μm was introduced between each shape. Using this design, we sought to predict unknown T specification given only the expression of phosphorylated myosin light chain (pMLC) and local cell density (Fig. 1 *B, iii*), reported as the fraction of each local region occupied by nuclei, using SVM learning (Fig. 1*C*).

Two-class learning was conducted identifying binary T+ and T− populations. We constructed three types of SVMs: a prediction (*i*) utilizing only density-normalized contractile protein expression, or

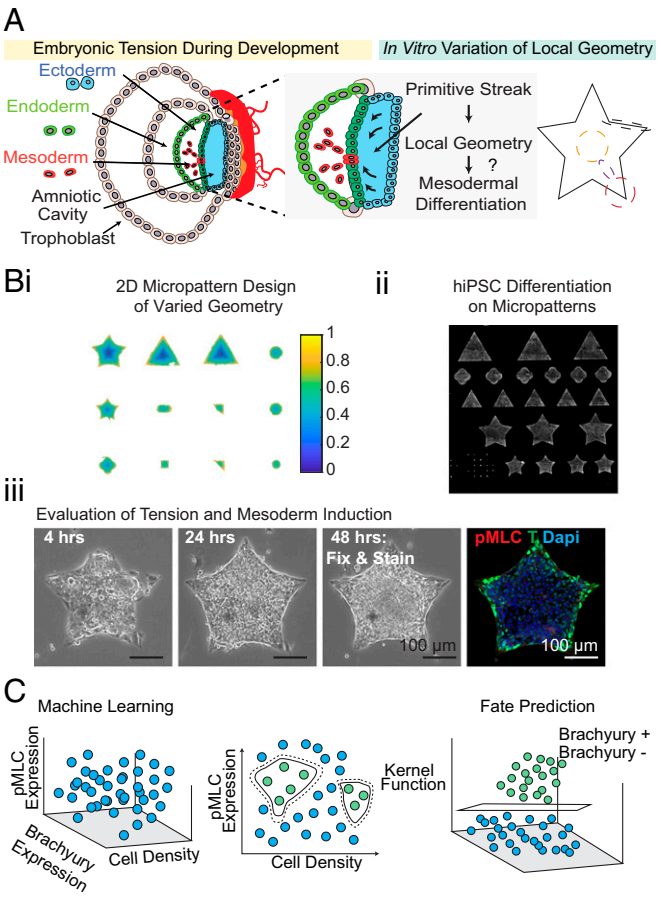

Fig. 1. SVM learning unveils cytoskeletal tension and density are strong predictors of T specification in unconfined culture. (*A*) Schematic of the experimental set up to control cell–cell and cell–matrix interactions to study the role of tension and early gastrulation events. (*B*) Work flow for the (*i*) design, (*ii*) seeding, and (*iii*) evaluation of the role of local geometry on mesodermal specification through micropatterning (representative immunofluorescence shown). (*C*) A schematic demonstrating SVM binary classification.

"Tension"; (*ii*) using only local cell density (reported as the fraction of a local region occupied by nuclei), or "Density"; and (*iii*) using both density and cytoskeletal tension, or "Dual." Each SVM was trained on a subset of the data for which the T classification was known. The SVM was then used to predict the classification for another subset based on the channels included, and performance statistics were calculated comparing the predicted values to the true labels. Cross-validation was performed in each case (*SI Appendix*, *SI Materials and Methods* and Figs. S12 and S13). The relative importance of Tension and Density may be interrogated based on the accuracy of the SVM classification using each channel independently or together.

Cytoskeletal Tension and Cell Density Are Strong Predictors of T Specification in Unconfined Culture. To test the power of this approach, we first investigated unconfined differentiation conditions using an established feeder free differentiation protocol that induces a mesoderm specification that can be further directed toward vascular commitment to ECs or pericytes (22, 23). First, we seeded hiPSCs on collagen IV-coated glass slides at low (50,000 cells per cm^2) and high (100,000 cells per cm^2) densities with the addition of ROCK inhibitor Y-27632 to promote stem-cell survival and adhesion (24). To test the role of actomyosin activity during mesoderm specification, media was replenished with or without ROCK inhibitor. After maintaining these culture

conditions for 48 h, cells were fixed and analyzed for T and pMLC. Cell interactions with the ECM-coated glass lead to the activation of Rho GTPases, which act to direct cytoskeletal protein assembly, cooperatively working to modulate the expression of myosin (10).

We found that cell density alone was an excellent predictor of T specification in unconfined culture, while contractile protein expression alone was a poorer predictor and only marginally improves accuracy when included in the Dual SVM for both pMLC and RhoA expression (*SI Appendix*, Fig. S2). In addition, the Tension/Density phase space was very narrow, and while Tension may be a poor predictor of T specification within that space, Tension was highest at low density where T expression was also highest. Additionally, we find that both RhoA, implicated in the regulation of cytoskeletal tension, and pMLC exhibit similar characteristics maintaining a qualitatively similar phase space for both labels. When Y-27632 was maintained in the media, we found a decrease in pMLC expression, and at high seeding densities, resulted in decreased proliferation and a lower density at the time of fixation (*SI Appendix*, Fig. S3). Consistent with our previous study investigating the effects of substrate stiffness and differentiation potential, we find a strong interplay between cell spreading, actomyosin contractility, and early mesodermal specification. Specifically, we find that cells plated at low density have increased pMLC expression, with a corresponding increase in T expression, corroborating additional published studies that have documented the role of cell density on mesodermal marker expression and tension (9, 24, 25).

SVM Learning Elucidates the Roles of Cytoskeletal Tension and Cell Density on T Expression. Aiming to understand the role of cytoskeletal tension in the fate determination of hiPSCs undergoing mesodermal induction, we cultured hiPSCs on collagen IV-coated micropatterned domains, ranging in size and geometric complexity. Culture conditions from the unconfined experiments were conserved, where 1×10^6 cells per micropatterned coverslip were seeded and allowed to differentiate for 48 h (Fig. 2*A* and Movies S1–S4). We found an increase in T expression around the periphery of control micropatterns with a corresponding increase in pMLC expression, a phenomenon conserved for a wide array of geometric configurations (Fig. 2 *B* and *C, i*). This spatial patterning was not observed on small patterns for which expression is largely uniform across the entire shape.

Using SVMs, we sought to predict unknown T specification given only pMLC/RhoA expression and local cell density (Fig. 2 *C, ii*). Under confinement, nuclear area decreased with increasing distance to the perimeter reported as the minimum distance between the centroid of the nucleus and the edge of the pattern. This trend may be attributed to density (Fig. 2*D*). The highest density on the patterns was present in a region near the edge; however, there are regions of low density near the edges as well, whereas the cell density was uniformly high in the centers of the patterns. To examine any shape dependence, the nuclear Eccentricity Ratio, defined as:

$$ER = \frac{\text{Area}}{\pi\left(\frac{1}{2}d\right)^2},$$

where Area is area of the nucleus and d is the maximum distance between any two points on the perimeter of the nucleus, was constructed. There was no observed dependence on seeding density in unconfinement or distance to the perimeter under confinement (Fig. 2*E*).

We found that mirroring the unconfined case, cell density, reported as the fraction of each local region occupied by nuclei, alone was able to predict T specification with high sensitivity and specificity (*SI Appendix*, Table S1), and tension alone was a less

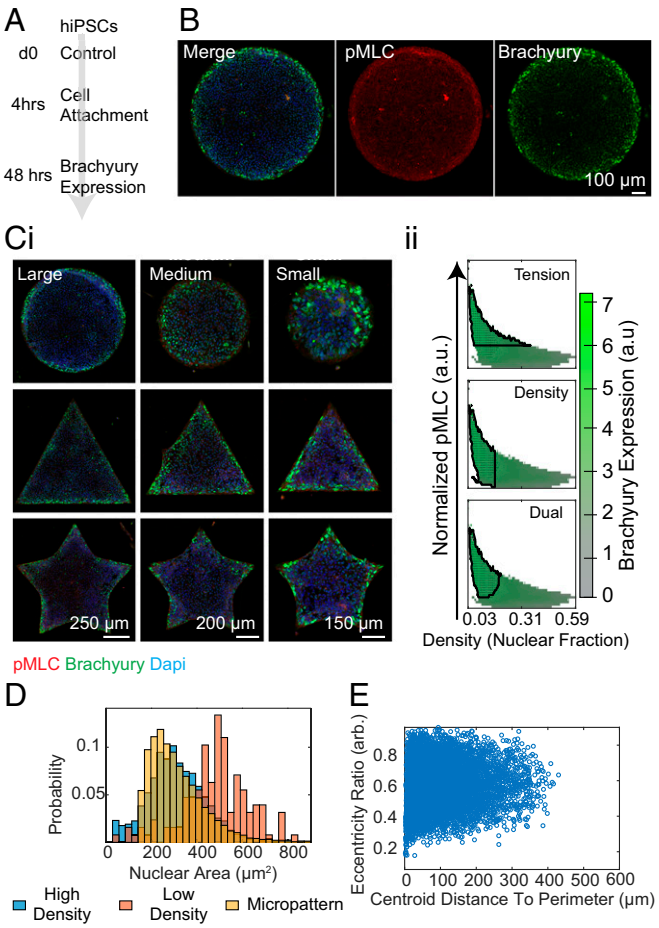

Fig. 2. Micropatterning induces mesodermal patterning. (*A* and *B*) Differentiation scheme under control micropattern conditions demonstrates an annulus of increased T and pMLC expression. (*C, i*) Spatial T and pMLC expression was conserved across a range of geometric configurations and micropattern sizes as shown by representative immunofluorescence images. (*C, ii*) Corresponding image analysis shows dependencies on local cell density and pMLC expression for T induction. (*D*) Distribution of nuclear area of cells across differentiation conditions. (*E*) Eccentricity Ratio of cells under confinement.

powerful predictor, only marginally improving specificity when included in the Dual classification. Here, the accuracy of each prediction is reported by the sensitivity and specificity of the classification. "Pixel Sensitivity" and "Pixel Specificity" refer to the unweighted statistics where each pixel in the phase space is presumed to come from an equal amount of contributing data, whereas "Sensitivity" and "Specificity" report the weighted results (*SI Appendix*, Table S1).

In the case of RhoA/ROCK inhibition, we find different behavior of the cells on the micropatterns than what we observed in unconfinement (Fig. 3 *A* and *B*). After the cells were allowed to adhere for 4 h in Y-27632, media was replaced with fresh Y-27632 for an additional 44 h before fixation. With the addition of Y-27632, cell condensation and spatial organization were diminished across varied micropattern size and geometry as previously reported (Fig. 3 *C, i*) (14). The SVM phase space was also perturbed under RhoA/ROCK inhibition (Fig. 3 *C, ii*). The performance of both Tension and Density as predictors of T specification was slightly hampered relative to control samples; however, when used in tandem, the predictive power was actually slightly increased (*SI Appendix*, Table S1). It should be noted that in addition to using Y-27632, we also attempted to disrupt microtubule polymerization. However, the addition of

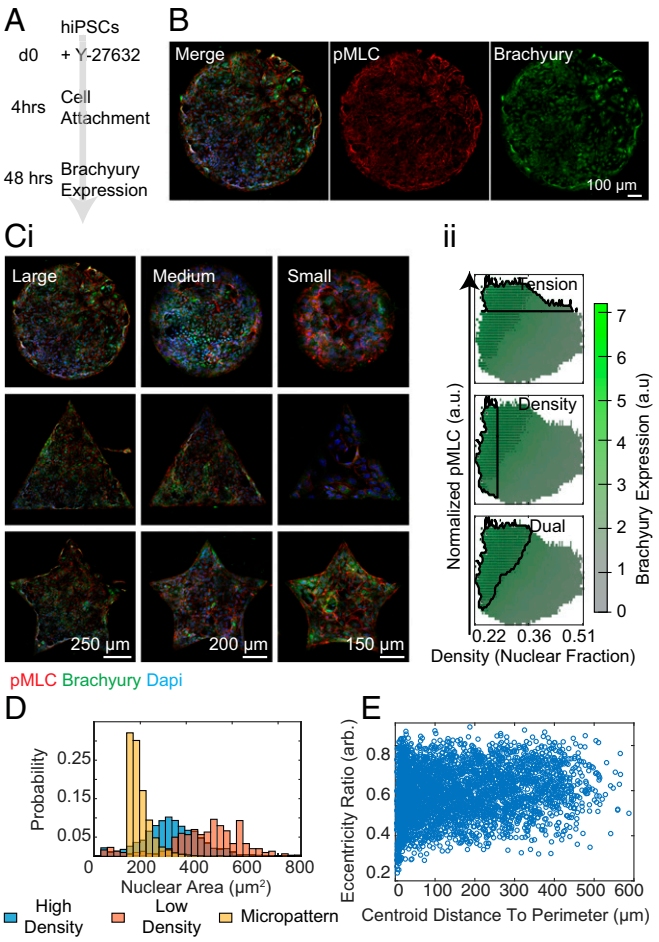

Fig. 3. Rock inhibition disrupts mesodermal patterning. (*A* and *B*) Differentiation scheme where micropatterns are treated with 10 μM Y-27632. (*C*) Micropatterns treated with (*i*) Y-27632 of different shapes and sizes and (*ii*) corresponding phase spaces and outlined SVM prediction. (*D*) Distribution of nuclear area across differentiation conditions. (*E*) Eccentricity Ratio of cells under confinement.

Nocodazole inhibited proper segmentation, as we observed extreme nuclear deformation and cell loss (*SI Appendix*, Fig. S4). Nuclear area showed qualitatively similar density dependence on and off the patterns (Fig. 3*D*), and again there was no change in eccentricity as a function of position on the patterns (Fig. 3*E*).

Overall, these results demonstrate the interplay between cell density and cytoskeletal tension as potential indicators of mesodermal differentiation efficiency and provide insight into the role of ECM availability in the self-organization of differentiated populations. Importantly, introducing unbiased SVM approaches allows for the prediction of T+ populations across multiple differentiation conditions and provides insight into maturation machinery. Specifically, with the addition of Y-27632, we found that cell density alone was not a reliable variable for predicting early mesodermal fate, highlighting the importance of tension in cell–cell interactions during maturation.

Early Mesoderm Patterning Predicts Vascular Specification. To investigate the effect of early mesoderm specification, evidenced by T expression on the micropattern domains, we extended differentiation on the micropatterns toward early vascular cell (EVC) populations based on our previous work (22, 23, 26). Briefly, cells were differentiated with and without temporary RhoA/ROCK inhibition for 48 h. After 2 d in the respective conditions, media was replaced for an additional 4 d without Y-27632. On day 6 of differentiation, the micropatterns were switched to an EVC-promoting media, consisting of VEGF and a TGFB-inhibitor to promote endothelial differentiation and suppress mesenchymal fate, respectively. After 12 d of culture, patterns were fixed and imaged for vascular endothelial cadherin (VECad) and smooth muscle protein 22-alpha (SM22α) to identify ECs and pericytes, respectively (Fig. 4*A*). In the control conditions, where Y-27632 was only added to promote attachment, we found spatially localized vascular derivatives as a function of micropattern geometry (Fig. 4*B*). With the maintenance of RhoA/ROCK inhibition at the onset of early mesoderm specification, spatial EVC organization is lost by day 12, leading to robust pericyte differentiation evidenced by SM22α expression (Fig. 4*C*).

We speculated that VECad expression on day 12 was consequential to the magnitude of density polarization on day 2 of differentiation (Fig. 3*F*). To this end, we quantified the degree of polarization by taking the ratio between the 75th percentile of the high-density region toward the edge of the patterns (maximum value of the shaded band) and the 25th percentile at the boundary of the patterns (minimum value of the shaded band). We hypothesized that when there is enhanced polarization on day 2, there is VECad expression within a small region of the Density/Distance-to-the-Perimeter phase space on day 12. On the other hand, we anticipated that when this ratio is low, demonstrating a lack of condensation on the boundaries, there will be minimal VECad expression post-EVC differentiation (Fig. 4*D*). Indeed, we found that in control conditions the degree of polarization was found to be 2.25 and 1.5 with Y-27632 (Fig. 4*D*).

Across the ensemble of micropatterns analyzed (*SI Appendix*, Table S1), regions of peak VECad and SM22α expression were at the edges of patterns under control conditions, with SM22α

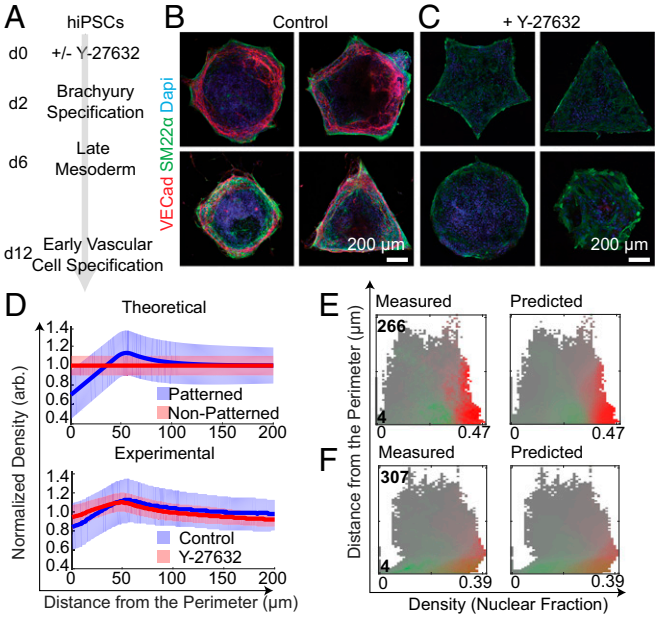

Fig. 4. SVM predicts spatial organization of EVCs on micropattern domains. (*A*) EVC differentiation protocol on micropatterns. (*B* and *C*) Representative images of control and Y-27632–treated day 12 micropatterns. (*D*, *Top*) Predicted EVC marker expression as a function of cell density and distance to the perimeter under micropatterned confinement. (*D*, *Bottom*) Experimental contribution of day 2 cell density and VECad expression between control and Y-27632–treated samples Shaded bands represent 50% of all data; median is represented by solid lines. Measured and predicted SVM landscapes for (*E*) control and (*F*) Y-27632 micropatterns for SM22α (green) and VECad expression (red) on day 12.

peak expression at densities slightly below the region where VECad expression was highest (*SI Appendix*, Fig. S14). The "Measured Landscape," indicating the percentile of high SM22α or VECad pixels (pixels that fall into the top 20% of all data) included at each point within the phase space, shows a clear division between high SM22α-expressing regions and high VECad-expressing regions (Fig. 4 *E, Left*). Specifically, VECad expression increased as a function of cell density (reported as the fraction of each local region occupied by nuclei) for all values of distance to the perimeter, whereas SM22α expression was higher at lower densities for larger distances to the perimeter. This region (in the upper left of the phase space) corresponding to low-density shapes were almost entirely VECad-negative and SM22α-positive (Fig. 4 *E, Left*). Furthermore, the "Predicted Landscape," calculated using SVMs, was an excellent replica of Fig. 4 *E, Left*, indicating that knowing cell density and distance to the perimeter of each pattern is sufficient to predict SM22α and VECad expression (Fig. 4 *E, Left* and *SI Appendix*, Fig. S5).

In contrast with Y-27632, a poorly separable Measured Landscape and similarly blurred Predicted Landscape resulted (Fig. 4 *E, Right* and *SI Appendix*, Fig. S14). The loss of spatial localization with the addition of RhoA/ROCK inhibition suggests an interplay between tension and cell density is important for pattern formation during vascular specification. Cumulatively, these results demonstrate the sensitivity of early mechanotransduction of hiPSCs on micropattern domains and its impact on vascular cell fate and self-organization under prolonged confinement.

The Mechanical Environment Regulates Vascular Fate. Here we created a platform to predict the roles of two broad variables on vascular lineage specification, cytoskeletal tension and cell density. These parameters are closely related with increased cell density leading to decreased tension; however, through the use of micropatterning, we are able to study geometries where density and tension may be independently modulated. We probed three possible mechanical environments: (*i*) low density and lack of cell–cell contact, (*ii*) high density with extensive cell–cell contact, and (*iii*) high density within confined micropatterns with areas of low cell–cell contact (edges) and high cell–cell contact (center) (Fig. 5*A*). As we have previously demonstrated that peak T expression occurs in 2 d under our mesoderm-inducing media (23), we stained these variable environments after 48 h of culture and assessed how each contributed to T specification. We found that all three cases induce T expression. In unconfined culture, increasing density leads to lower T intensity, whereas in confined culture increased density toward the edge of the micropatterns corresponded to an annulus of high T expression. To directly interrogate the role of tension on T expression and spatial organization, we introduced a small-molecule inhibitor to disrupt cellular mechanotransduction and found modest effects in unconfined culture but a drastic reduction in spatial organization on micropatterns.

Our previous two-step differentiation protocols, where cells are passaged following mesoderm induction, have demonstrated how cell-seeding density impacts the downstream efficiency of EC and pericyte specification (20). Here, where cells are maintained in the differentiation niche without intermediate passaging steps, we show that decreased cell density leads to a uniform population of high SM22α-expressing pericytes (*SI Appendix*, Fig. S6). While initial high cell seeding permits disordered, mixed populations of both pericytes and ECs in unconfined cultured, prolonged micropatterned culture leads to vascular organization during differentiation. After 12 d of differentiation, we found structures that mimicked native vasculature with an outer ring of pericytes, immediately adjacent to an inner layer of VECad-expressing ECs. Interestingly, at the center of these domains, both SM22α and VECad expression was minimal. This phenotype was only observed in micropatterns large enough to support two distinct "edge" and "center" niches, similar to cardiac

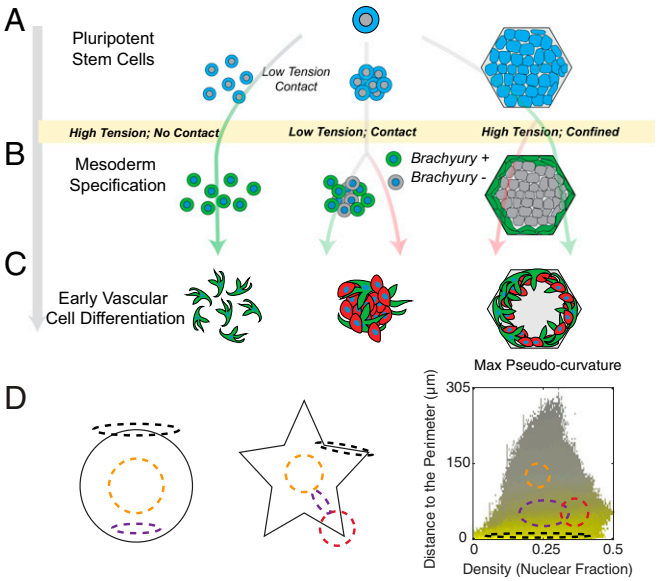

Fig. 5. Balancing cytoskeletal tension and cell–cell contact mediates vascular differentiation. (*A*) Tipping the balance between cytoskeletal tension and cell–cell contact leads to diverse differentiation outcomes. (*B*) On day 2 of differentiation, all microenvironments display T specification, though expression is strongly determined by cell density. (*C*) On day 12, micropatterened domains display concentric rings of high SM22α and VECad-expressing cells. (*D*) Conceptual dependence of local geometry and density distribution under confinement.

chambers generated on micropatterned domains (14). Using image processing and SVM learning for T and EVC specification, we suggest this organization is driven in part by varying degrees of cytoskeletal tension. We propose that cells that experience high tension at the exterior of a micropatterned colony express high levels of T at day 2 and SM22α by day 12, while cells with high cell–cell contact directly adjacent to this outer layer have a slightly lower tension and preferentially differentiate into endothelium, suggestive of the multicellular assembly in a vascular conduit (Fig. 5 *B* and *C*). This theory can be corroborated by our studies with temporary mechanotransduction inhibition, through the reduction of RhoA/ROCK activity with Y-27632.

Under temporary addition of Y-27632, cells appeared larger at day 2 and appear to have a lower proliferation capacity even 12 d postdifferentiation. Control patterns rapidly proliferate, growing out of plane on many patterns into 3D spheroids (*SI Appendix*, Fig. S7), while those treated with Y-27632 almost exclusively remain as monolayers. Perhaps most importantly, patterns treated with Y-27632 showed far reduced spatial organization, and almost no patterns were observed that display the concentric rings of SM22α and VECad expression revealed in controls (*SI Appendix*, Fig. S8). In addition, Y-27632 gently perturbs T expression levels and spatial organization on day 2 and vividly disrupts the spatial patterning observed in day 12. We suggest vascular formation is driven in part by a simple scheme. Cells experiencing high cytoskeletal tension at the exterior of a colony express high levels of SM22α exhibiting a pericyte-like phenotype. Cells with high cell–cell contact directly adjacent to the outer layer but experiencing lower tension express high levels of VECad, portraying an endothelial phenotype.

We propose a model in which local geometries can direct self-organization events. This is illustrated and described as follows (Fig. 5*D*): In this system, we observed four different types of domains; an edge of a pattern (black); the region of increased density toward the edge of a pattern—an annulus in the case of a circle (purple), the center of a pattern (yellow), and a region of increased density toward the edge of patterns with corners—and

thus two neighboring edges—subjected to higher tension deeper into the center of the pattern (red). In a previous study, we tracked other mesodermal markers along our differentiation scheme, showing the temporal expression of markers including KDR, GATA-2, MESP-1, and SNAIL (26). We view the current study as a robust computational foundation to explore the temporal/spatial expression of these markers in the context of cytoskeletal tension, allowing more insight into mechanical regulation of vascular specification.

Conclusions

Our results demonstrate the potential for integrating micropatterning technology with image-processing and machine-learning algorithms to evaluate differentiation parameters as they relate to early and downstream lineage specification. We show that the seeding of hiPSCs as single cells on micropatterns, which vary in geometric complexity, leads to germ layer patterning, specifically an annulus (in the case of a circular pattern) of T+ cells after 48 h of differentiation. While this phenomenon has been largely attributed to the presence of soluble cues, we show that reduction of cytoskeletal tension perturbs this system in a manner that is predicted from SVM analysis. Next, by continually differentiating hiPSCs to vascular cells, we show that early tension triggers efficient T specification, further guiding spatial vascular fate organization across an array of geometric configurations. These results suggest early differentiation events, specifically those impacted by cytoskeletal tension, induce a specific transcriptional window where the presentation of additional cues to coax lineage specification after this critical time point is ineffective in driving endothelial differentiation. The combination of patterning and SVM learning offers the capacity to engineer specific outputs resulting from different vascular differentiation outcomes by tuning early tension and density inputs. Collectively, these results show the applicability of micropatterning technology for studying pattern formation in early and late-stage differentiation events. We foresee the use of SVM with other tools, including gene editing technology, creating a pipeline where live reporter systems containing multiple gene alterations can be used in tandem to mechanistically understand the interplay between cell–cell communication and physical cues in stem-cell differentiation.

Materials and Methods

Detailed materials and methods are provided in *SI Appendix, SI Materials and Methods*.

hiPSC Differentiation and Immunofluorescence Staining. Activated micropatterned glass coverslips (CYTOO) were coated with collagen IV (Corning). hiPSCs were seeded at 1×10^6 per micropatterned coverslip. After 4 h of attachment, Y-27632 was removed or retained as outlined in the text, and fresh Diff Media was replaced. After 48 h of culture, cells were fixed for immunofluorescence staining. To induce EVC specification, seeded micropatterns were cultured in Diff Media that on day 6 was switched to EC Diff Media (15, 22, 23, 26). Cells cultured on micropatterned surfaces were fixed and stained (*SI Appendix*, Table S2). Images were acquired using a Zeiss 780 confocal microscope.

SVM Learning. Immunofluorescence images were smoothed to obtain local population averages. First, nuclear masks were made alongside identifying unconfined or patterned domains. Each channel was averaged within discs of a few cell diameters in radius. For day 2 images, the three channels of interest for each experiment were mean pMLC/RhoA normalized by cell density, cell density, and T expression. For day 12, the channels of interest were cell density with the addition of distance to the perimeter of the pattern, SM22α, and VECad. For day 2, two-class learning was accomplished between low-T and high-T (0.5 SDs above the mean) regions. For day 12, multiple SVMs were trained to 100 masks for both the SM22α and VECad channels, predicting each percentile of the expression landscape. Performance statistics (sensitivity and specificity) were calculated. For day 2, the predictive power of only cell density, only pMLC/RhoA expression, and dual channels were compared.

ACKNOWLEDGMENTS. We thank Bria Macklin for helpful discussions and technical advice. This work was supported by the National Research Service Award (NRSA) F31 Predoctoral Fellowship F31HL134329 (to Q.S.), Maryland Stem Cells Research Fund Grant MSCRFI-2784, Established Investigator Award (EIA) from American Heart Association Grant 15EIA22530000 (to S.G.), and NCI Physical Sciences-Oncology Center Grant U54CA210173 (to S.G. and S.S.).

1. Lian X, et al. (2013) Directed cardiomyocyte differentiation from human pluripotent stem cells by modulating Wnt/β-catenin signaling under fully defined conditions. *Nat Protoc* 8:162–175.
2. Patsch C, et al. (2015) Generation of vascular endothelial and smooth muscle cells from human pluripotent stem cells. *Nat Cell Biol* 17:994–1003.
3. Wichterle H, Lieberam I, Porter JA, Jessell TM (2002) Directed differentiation of embryonic stem cells into motor neurons. *Cell* 110:385–397.
4. Noble WS (2006) What is a support vector machine? *Nat Biotechnol* 24:1565–1567.
5. Ramaswamy S, et al. (2001) Multiclass cancer diagnosis using tumor gene expression signatures. *Proc Natl Acad Sci USA* 98:15149–15154.
6. Treiser MD, et al. (2010) Cytoskeleton-based forecasting of stem cell lineage fates. *Proc Natl Acad Sci USA* 107:610–615.
7. Morin RD, et al. (2008) Application of massively parallel sequencing to microRNA profiling and discovery in human embryonic stem cells. *Genome Res* 18:610–621.
8. Perestrelo T, et al. (2017) Pluri-IQ: Quantification of embryonic stem cell pluripotency through an image-based analysis software. *Stem Cell Reports* 9:697–709.
9. Warmflash A, Sorre B, Etoc F, Siggia ED, Brivanlou AH (2014) A method to recapitulate early embryonic spatial patterning in human embryonic stem cells. *Nat Methods* 11: 847–854.
10. Nayak RC, Chang K-H, Vaitinadin N-S, Cancelas JA (2013) Rho GTPases control specific cytoskeleton-dependent functions of hematopoietic stem cells. *Immunol Rev* 256: 255–268.
11. Tewary M, et al. (2017) A stepwise model of reaction-diffusion and positional information governs self-organized human peri-gastrulation-like patterning. *Development* 144: 4298–4312.
12. Etoc F, et al. (2016) A balance between secreted inhibitors and edge sensing controls gastruloid self-organization. *Dev Cell* 39:302–315.
13. Smith Q, Stukalin E, Kusuma S, Gerecht S, Sun SX (2015) Stochasticity and spatial interaction govern stem cell differentiation dynamics. *Sci Rep* 5:12617.
14. Ma Z, et al. (2015) Self-organizing human cardiac microchambers mediated by geometric confinement. *Nat Commun* 6:7413.
15. Kusuma S, Smith Q, Facklam A, Gerecht S (2017) Micropattern size-dependent endothelial differentiation from a human induced pluripotent stem cell line. *J Tissue Eng Regen Med* 11:855–861.
16. Azzolin L, et al. (2014) YAP/TAZ incorporation in the β-catenin destruction complex orchestrates the Wnt response. *Cell* 158:157–170.
17. Engler AJ, Sen S, Sweeney HL, Discher DE (2006) Matrix elasticity directs stem cell lineage specification. *Cell* 126:677–689.
18. McBeath R, Pirone DM, Nelson CM, Bhadriraju K, Chen CS (2004) Cell shape, cytoskeletal tension, and RhoA regulate stem cell lineage commitment. *Dev Cell* 6: 483–495.
19. Wen JH, et al. (2014) Interplay of matrix stiffness and protein tethering in stem cell differentiation. *Nat Mater* 13:979–987.
20. Boraas LC, Guidry JB, Pineda ET, Ahsan T (2016) Cytoskeletal expression and remodeling in pluripotent stem cells. *PLoS One* 11:e0145084.
21. Abagnale G, et al. (2017) Surface topography guides morphology and spatial patterning of induced pluripotent stem cell colonies. *Stem Cell Reports* 9:654–666.
22. Chan XY, et al. (2015) Three-dimensional vascular network assembly from diabetic patient-derived induced pluripotent stem cells. *Arterioscler Thromb Vasc Biol* 35: 2677–2685.
23. Kusuma S, et al. (2013) Self-organized vascular networks from human pluripotent stem cells in a synthetic matrix. *Proc Natl Acad Sci USA* 110:12601–12606.
24. Bhadriraju K, et al. (2007) Activation of ROCK by RhoA is regulated by cell adhesion, shape, and cytoskeletal tension. *Exp Cell Res* 313:3616–3623.
25. Evans ND, et al. (2009) Substrate stiffness affects early differentiation events in embryonic stem cells. *Eur Cell Mater* 18:1–13, discussion 13–14.
26. Smith Q, et al. (2017) Compliant substratum guides endothelial commitment from human pluripotent stem cells. *Sci Adv* 3:e1602883.